Published in final edited form as:
ACS Nano. 2013 July 23; 7(7): 5684–5693. doi:10.1021/nn401911k.

The Effect of Injection Routes on the Biodistribution, Clearance and Tumor Uptake of Carbon Dots

Xinglu Huang[†], **Fan Zhang**[†,‡], **Lei Zhu**[†,‡], **Ki Young Choi**[†], **Ning Guo**[†], **Jinxia Guo**[†,‡], **Kenneth Tackett**[¶], **Parambath Anilkumar**[¶], **Gang Liu**[‡], **Qimeng Quan**[†], **Hak Soo Choi**[§], **Gang Niu**[†], **Ya-Ping Sun**[¶], **Seulki Lee**[†], and **Xiaoyuan Chen**[†,*]

[†]Laboratory of Molecular Imaging and Nanomedicine (LOMIN), National Institute of Biomedical Imaging and Bioengineering (NIBIB), National Institutes of Health (NIH), Bethesda, Maryland, 20892, United States

[‡]Center for Molecular Imaging and Translational Medicine, School of Public Health, Xiamen University, Xiamen 361005, China

[¶]Department of Chemistry and Laboratory for Emerging Materials and Technology, Clemson University, Clemson, South Carolina 29634, United States

[§]Division of Hematology/Oncology, Department of Medicine, Beth Israel Deaconess Medical Center, Boston, Massachusetts 02215, United States

Abstract

The emergence of photoluminescent carbon-based nanomaterials has shown exciting potential in the development of benign nanoprobes. However, the *in vivo* kinetic behaviors of these particles that are necessary for clinical translation are poorly understood to date. In this study, fluorescent carbon dots (C-dots) were synthesized and the effect of three injection routes on their fate *in vivo* was explored by using both near-infrared fluorescence (NIRF) and positron emission tomography (PET) imaging techniques. We found that C-dots are efficiently and rapidly excreted from the body after all three injection routes. The clearance rate of C-dots is ranked as: intravenous > intramuscular > subcutaneous. The particles had relatively low retention in the reticuloendothelial system (RES) and showed high tumor-to-background contrast. Furthermore, different injection routes also resulted in different blood clearance patterns and tumor uptakes of C-dots. These results satisfy the need for clinical translation and should promote efforts to further investigate the possibility of using carbon-based nanoprobes in a clinical setting. More broadly, we provide a testing blueprint for *in vivo* behavior of nanoplatforms under various injection routes, an important step forward towards safety and efficacy analysis of nanoparticles.

Keywords

Biodistribution; carbon dots; clearance; injection routes; translation; tumor uptake

Luminescent semiconductor quantum dots (QDs) have generated much excitement for a wide variety of promising applications in biolabeling and bioimaging fields.[1–8] However, the known toxicity and potential environmental hazard of these inorganic nanomaterials containing heavy metals such as cadmium limit their widespread use and *in vivo*

*Corresponding Author: Shawn.Chen@nih.gov.

SUPPORTING INFORMATION. Materials and methods section and additional figures. This material is available free of charge *via* the Internet at http://pubs.acs.org.

applications in humans.[9–13] The emergence of photoluminescent carbon-based nanomaterials provides an exciting opportunity in the search for benign (nontoxic) alternative fluorescent nanomaterials, and might offer great potential for optical imaging and related biomedical applications. These surface-functionalized carbon nanodots (C-dots) with ultra-small sizes were found to be physicochemically and photochemically stable.[14] Combined with their well-defined, ultrafine dimensions and a variety of simple, fast, and cheap synthetic routes available,[15–23] C-dots provide an encouraging technological platform as an alternative to other carbon-based nanomaterials such as fullerenes, nanodiamonds, and carbon nanotubes, and are expected to have wide applications in preclinical and potentially clinical studies.[24]

Recently, Liu's group reported that C-dots do not have noticeable signs of toxicity in treated animals,[25] demonstrating the feasibility for *in vivo* applications. The successful translational of nanoparticles-based biomaterials not only requires nanoparticles (NPs) with well-controlled *in vivo* behavior,[26,27] but also possess the lowest possible likelihood of toxicity. The US Food and Drug Administration (FDA) has demanded that the agents injected into the human body, especially diagnostic agents, should be cleared completely in a reasonable period of time,[28] that such agents should not accumulate in the body and that their exposure time should be minimized. To date, the key determinants of NP biodistribution and clearance focus on the properties of NPs, such as the chemical composition, size, shape, and surface charge.[28–31] However, very few reports pay attention to factors applied in the clinic, such as injection or exposure routes, which are necessary for clinical translation of nanoformulations. Several studies reported significant differences in NP toxicity based on different exposure routes.[32,33] Although meaningful progress has been made in the synthesis strategy of C-dots, there is no report of C-dots that can target a disease state, and can be efficiently cleared from the body after different injection routes.

RESULTS AND DISCUSSION

Fabrication and characterization of near-infrared C-dots

Herein, we prepared near-infrared fluorescent C-dots (Fig. 1A), by coupling the nanoparticles (NPs) with near-infrared dye ZW800, to track their *in vivo* fates and the effect of tumor uptake after three injection routes: intravenous (i.v.), subcutaneous (s.c.) and intramuscular (i.m.), respectively. In a typical preparation, the C-dots were firstly synthesized according to a previously reported method.[21,22,34] Subsequently, surface passivation of C-dots was performed by reacting with diamine-terminated oligomeric poly(ethylene glycol). Three major purposes were implemented in the surface passivation process: 1) generation of bright luminescence;[21] 2) improvement of hydrophilicity and stability; 3) surface functionalization of C-dots. TEM imaging shows ultra-small surface passivated C-dots of ~3 nm (Fig. 1B).

The photoluminescence from C-dots is most likely attributed to the presence of surface energy traps that become emissive upon stabilization as a result of surface passivation.[21] Currently, a major reason limiting *in vivo* applications of C-dots is their low quantum yields in the near-infrared (NIR) region (650–900 nm), an ideal tissue fluorescence imaging window with low tissue absorption and scattering.[35–37] To improve the emission ability of C-dots in the NIR region, ZW800 (excitation ~770 nm, emission ~795 nm) was introduced onto C-dots by conjugating the dye NHS ester with amino groups on the C-dots, to make ZW800 labeled C-dots (C-dot-ZW800). There are about 20 dye molecules per particle on average as estimated by quantifying the fluorescence intensity and absorbance values of ZW800 before and after conjugation. C-dot-ZW800 has the absorption peaks at approximately 420 nm (C-dots) and 770 nm (ZW800) (Fig. 2A), and two emission peaks at approximately 510 nm and 800 nm after excitation, respectively (Fig. 2B). The imaging

ability of C-dot-ZW800 in the visible and in the NIR range was also shown after excitation at different wavelengths by a Maestro all-optical imaging system (Fig. 2C). Furthermore, the low fluorescence background of C-dot-ZW800 was shown in different biological fluids, such as fetal bovine serum (FBS), blood, urine and tissue lysate (Supporting information Fig. S1). To better study the *in vivo* kinetics of C-dots, we also explored the fluorescence stability and particle stability of C-dot-ZW800. The fluorescence stability of C-dot-ZW800 was observed in the urine and blood. As shown in Supporting information Fig. S2, the fluorescence signals derived from C-dots and ZW800 were virtually unaltered over extended incubation time.

In our previous study, we demonstrated that the naked C-dots bear negtive charges due to the existence of –OH/-COOH groups on the surface, with zeta potential of −24 mV.[38] After passivation with PEG-amine, the zeta potential of C-dots was −14.3 ± 2.8 mV, further modification with ZW800 dye molecules,[39] the zeta potential of C-dot-ZW800 became −9.4 ± 4.6 mV. Dynamic light scattering (DLS) is a notoriously inaccurate technique for the characterization of weakly scattering colloids with small sizes, such as these C-dots, in contrast with highly scattering materials like gold. To better define the hydrodynamic diameter (HD) of particles, gel-filtration chromatography (GFC) system was used to characterize small sized NPs with various coatings according to previous reports.[29,40] First, the protein standards were analyzed using GFC, including M1 (thyroglobulin; 669 kDa, 18.8 nm HD), M2 (γ-globulin; 158 kDa, 11.9 nm HD), M3 (ovalbumin; 44 kDa, 6.13 nm HD), M4 (myoglobin; 17 kDa, 3.83 nm HD), and M5 (vitamin B12; 1.35 kDa, 1.48 nm HD) (Fig. 2D). Subsequently, a standard curve of HD *vs.* retention time was established, and the HD of C-dot-ZW800 was calculated to be 4.1 nm based on its GFC retention time (Fig. 2E). To measure whether there is potential adsorption of serum proteins, C-dot-ZW800 were incubated in PBS, fetal bovine serum (FBS), or mouse urine for 1 h at 37 °C before loading onto the GFC column. As shown in Fig. 2F, slight changes in the peak shape and retention time were found, indicating the possibility of adsorption of plasma protein onto the surface of C-dot particles.

Blood circulation of particles by three injection routes

Before the NPs can be ready for clinical translation, a good understanding of their *in vivo* behavior is needed to minimize their potential toxicity. First, we studied the *in vivo* kinetics of C-dots by different injection routes. After injection of C-dots by three routes (i.v., s.c. and i.m.), venous blood samples were collected at the indicated time points and subsequently analyzed by a Maestro all-optical imaging system. As shown in Fig. 3, blood clearance rates of C-dot-ZW800 are rather different after different injection routes, according to the analysis of fluorescence signals from ZW800 dyes. The particle concentration in blood within 1 h dramatically decreased after i.v. injection (Fig. 3A, top), while it was initially increased after s.c. (Fig. 3A, middle) and i.m. injection (Fig. 3A, bottom) and then plateaued after 30 min and 20 min post-injection, respectively. The quantitative analysis found that the particle fluorescence signal in blood at 1 min after i.v. injection was 17.3 ± 4.6 fold higher than 60 min (n = 4/group, Fig. 3B). On the other hand, both s.c. and i.m. injection groups showed lower particle concentration at 1 min post-injection than that at 60 min by 4.4 ± 1.3 fold and 9.6 ± 2.6 fold, respectively. To further confirm the particle concentration, representative fluorescence images of the collected blood at indicated time points after i.v. injection of C-dot-ZW800 were collected for C-dot and ZW-800 (Supporting information Fig. S3). The same trend of blood clearance was observed for C-dots and ZW800, implying that the conjugated ZW800 dye molecules were not detached from the C-dot particles. We observed that the retention time of C-dot-ZW800 in blood after s.c. and i.m. injection was significantly higher than that after i.v. injection, signifying the impact of injection route on the *in vivo* behaviors of given nanoparticles such as C-dots. It is speculated that the rapid

blood clearance of C-dot- ZW800 might be due to serum protein adsorption onto the particle surface, leading to rapid opsonization followed by removal from the reticuloendothelial system.

Biodistribution of C-dot nanoparticles by three injection routes

To minimize the toxicity of NPs, it is necessary to account for and completely remove all NPs from the body within a reasonable period of time. After being introduced into a living subject, NPs are typically metabolized *via* two major routes, the liver (into bile) and the kidneys (into urine).[41] To fully understand the clearance route of C-dots, organs were collected at 1 h and 24 h after C-dot administration, and the biodistribution of particles was analyzed by quantitative *ex vivo* imaging. As shown in Fig. 4A and Supporting information Fig. S4A, majority of C-dot-ZW800 particles were accumulated in the kidneys at 1 h after injection *via* all three routes, only small amount went to the liver. The signal of C-dot-ZW800 in the kidneys at 1 h time point was quantified and ranked based on the injection routes as: i.m. > s.c. > i.v. (Supporting information Fig. S4B). After 24 h, no significant signal was detected in any organ, suggesting that the particles were all cleared out of the body regardless of the injection route (Supporting information Fig. S4C).

To further validate the biodistribution results obtained from optical imaging, we also employed positron emission tomography (PET) imaging to visualize and quantify the *in vivo* kinetics of the C-dots. The biodistibution of ^{64}Cu-C-dot measured by region of interest (ROI) analysis showed very similar pattern to that obtained from optical imaging (Fig. 4B). At 24 h post-injection of ^{64}Cu-C-dot, the mice were euthanized and major organs and tissues including blood, muscle, liver, kidneys, spleen, heart and lung were harvested and measured by gamma counting, revealing less than 1%ID/g radioactivity in any organ measured in all three injection routes (Fig. 4C), indicating low accumulation of C-dots in the reticuloendothelial system (RES) and rapid clearance from the body. Based on these results, it was concluded that C-dots were mainly excreted *via* the renal route into urine.

Urine clearance of particles by three injection routes

Urine clearance analysis of C-dots after three injection routes was further performed in order to evaluate the *in vivo* behaviors of C-dots. The bladder of each mouse after administration of C-dot-ZW800 was exposed and imaged at the indicated time points. The signal of C-dot-ZW800 was subsequently quantified to acquire a clearance curve. From Fig. 5A and B, a rapid clearance is observed by i.v. injection and the signal in the bladder was plateaued 10 min after administration. I.v. injection of C-dots displayed much faster urine clearance than the s.c. and i.m. injection route within 10 min post-injection, respectively. To confirm the urine clearance of particles, bladder images were also acquired based on C-dot emission over time (Supporting Information S5). The urine displayed high background in the visible region, making it unsuitable for signal quantification. However, the signal from C-dot emission demonstrated the same trend of urine clearance as ZW800 emission, again indicating that the ZW800 fluorescence signal reflects C-dot-ZW800. The urine activity was also quantified by PET imaging (Fig. 5C), which was in good accordance with the NIR fluorescence imaging results (Fig. 5D). The amount of signals (both quantified from ZW800 fluorescence and ^{64}Cu radiolabel) in the urine within 1 h postinjection of ^{64}Cu-C-dot-ZW800 showed the pattern of i.v. > i.m. > s.c., in accordance with the clearance rate from the blood.

Accumulation of particles at injection sites

Besides the accumulation in the RES, it is possible that the NPs accumulate at the injection site after s.c. and i.m. administration (Fig. 6A). For s.c. and i.m. injection, most particles initially retained at the injection site have disappeared by 24 h postinjection. Quantitative

analysis indicates that the signals at s.c. and i.m. injection site at 24 h time point were 92.3 ± 10.2 % and 99.1 ± 9.7 % lower than those at 1 min post-injection, respectively (Fig. 6B). These results elucidate that the NPs do not accumulate at the injection site and instead rapidly enter the blood circulation.

Tumor uptake of particles by three injection routes

For cancer nanomedicine applications, it is desirable for NPs to have prominent and prolonged tumor uptake. C-dot-ZW800 particles were injected *via* three injection routes into athymic nude mice bearing subcutaneous SCC7 tumors. The images were acquired and analyzed on a Maestro all-optical imaging system. At 2 h post-injection, tumor was easily distinguishable from surrounding normal tissue in all three groups and the tumor signal remained high over time (Fig. 7A). In addition to the homogeneous uptake of C-dots in the solid tumors, most of the remaining C-dot-ZW800 were excreted through renal filtration (red arrow), as shown by high tumor-to-background ratio and low level of fluorescence in other tissues and organs. The i.v. group and s.c. group exhibited higher fluorescence signal in the tumor area than the i.m. group at 2 h postinjection ($p < 0.05$) (Fig. 7B). The s.c. group also showed somewhat stronger signal than the i.v. group in the tumor at 2, 4 and 24 h post-injection ($p > 0.05$), presumably due to the slower blood clearance of C-dots *via* s.c. than i.v. injection. The imaging results were further confirmed by *ex vivo* microscopic imaging of the frozen tissue slices obtained from mice sacrificed at 2 h post-injection (Fig. 7C). Co-localization of C-dots and ZW800 in the tissue slices again excluding the possibility of dissociation of ZW800 from the C-dot-ZW800 conjugate.

In the present study, we found that C-dot-ZW800 particles were cleared mainly through the kidneys (into urine) and not the liver and spleen (Fig. 4). NPs are often trapped in the RES (mainly liver and spleen) by macrophages, and PEGylation greatly reduces trapping by the RES compared with the naked NPs. It has been reported that for PEGylated QDs, the hydrodynamic diameter has to be less than 5.5 nm for efficient renal excretion,[28–30,42] with clearance efficiency decreases as hydrodynamic diameter increases. Our water-soluble C-dots with core size of 3 nm and HD of 4.1 nm after PEGylation and ZW800 coupling led to rapid and efficient elimination of particles from the body *via* urinary excretion.

In clinical applications, different injection routes can be applied to fit special purposes, such as tumor targeting, long circulation or ease of use by the physicians. In this study, we illustrate that efficient clearance of C-dots is implemented not only after i.v. injection but also after s.c. and i.m. injection with no significant accumulation at the injection sites over time (Fig. 4 and 6). Owing to the presence of different biological barriers, the blood clearance and urine accumulation rate follows the order of i.v. > i.m. > s.c. (Fig. 3 and 5). Furthermore, tumor uptake of C-dots by s.c. and i.v. injection was higher than that by i.m. injection. This is probably due to the interplay among circulation time, clearance rate and the concentration of particles retained in the tumor *via* different injection routes.[28] For example, we showed that the blood clearance of C-dots after i.v. injection was faster than the other two injection routes (Fig. 5), which in turn could lead to reduced tumor retention. Thus, the *in vivo* behaviors of C-dots, such as the circulation time, major organ accumulation and passive tumor targeting can be easily controlled by the injection route. Overall, C-dots appear to have great potential as a nanoplatform for preclinical biomedical research and translation into clinic for optical imaging-guided surgery.

It is of note that while 2D fluorescence reflectance imaging used in this study is useful for qualitative and comparative analyses, it is unable to provide quantitative information, and it also does not allow for the assessment of C-dot accumulation in deeper-seated tissues. 3D fluorescence molecular tomography (FMT), based on volumetric reconstruction of the concentration of optical imaging agents, is generally considered to be able to overcome

some of the shortcomings associated with 2D optical imaging and to enable more quantitative and more in-depth analyses.[43] Combining anatomical μCT with FMT may be applied in the future to noninvasively assess the biodistribution of C-dot-ZW800 conjugate in addition to radiolabeled C-dot-ZW800.

CONCLUSION

In summary, we explored the effects of different injection routes on blood circulation, biodistribution, urine clearance and passive tumor uptake of C-dots. The C-dot-ZW800 conjugate was specifically designed to possess several significant features: NIR fluorescence emission, high stability *in vivo*, rapid renal clearance and effective passive tumor targeting. Our studies suggest that the injection route affects rate of blood and urine clearance, the biodistribution of C-dots in major organs and tissues, and tumor uptake over time. These characteristics make C-dot-based nanoprobes a viable candidate for clinical translation. We hope this study will lay the foundation for testing and designing targeted NPs with optimal exposure routes to control biodistribution, elimination from the body and tumor targeting – key criteria for safety approval and clinical translation.

METHODS

Synthesis and surface passivation of C-dots

Functionalized C-dots were synthesized according to previous reports.[21,34,44] Briefly, the C-dots were synthesized *via* laser ablation of a carbon target in the presence of water vapor with argon. Then, diamine-terminated oligomeric poly(ethylene glycol) $H_2NCH_2(CH_2CH_2O)_nCH_2CH_2CH_2NH_2$ (n = 35, M.W. ≈ 1,500, PEG_{1500N}) was used to react with the C-dots for surface passivation. In a typical reaction, PEG_{1500N} (200 mg, 0.13 mmol) was mixed with an acid-treated particle sample, and the mixture was heated to 120 °C for 72 h. After the reaction, the mixture was cooled to room temperature and dispersed in water, followed by centrifugation for 30 min. The supernatant containing C-dots was collected for further functionalization. The resulting particles were observed by transmission electron microscopy (TEM). The zeta potential of the particles was measured using a SZ-100 Nano Particle analyzer (Horiba Scientific).

Labeling of C-dots with near-infrared dye ZW800 and PET isotope ^{64}Cu

The near-infrared dye ZW800[35] was conjugated with C-dots by reaction between the amino groups of C-dots and the NHS ester of ZW800. To remove free PEG before conjugation, the samples were purified by dialysis membrane (M.W. ~3500) in a PBS solution for 5 days by changing fresh solution every 6–12 h. In a typical reaction, the C-dots (20 mg) were labeled with ZW800 (1 mg) in 10 mL borate buffer (pH = 9.0) solution. The reaction mixture was stirred at room temperature for 4 h and then purified by PD-10 desalting column (GE healthcare). To make sure that free PEG-dye conjugate was completely removed, the product was further purified by dialysis membrane (M.W. ~3500) in a PBS solution for 3 days by changing fresh solution every 6–12 h. Finally, the C-dot-ZW800 was concentrated into 5 mL PBS and collected by a centrifugal filter (3k cutoff, Millipore). The UV-Vis and fluorescence spectra of particles were recorded on a Genesys 10s UV-Vis spectrophotometer (Thermo, IL) and an F-7000 fluorescence spectrophotometer (Hitachi, Japan), respectively.

For ^{64}Cu labeling, the amino groups of C-dots were firstly conjugated with DOTA-NHS ester (Macrocyclics). Briefly, 5 mg C-dots were reacted with 0.5 mg DOTA-NHS ester in 2 ml borate buffer (pH = 9.0). The mixture was stirred at room temperature for 4 h and subsequently purified by PD-10 desalting column. The product was concentrated into 0.5 mL PBS with a centrifugal filter. Then, the C-dot-DOTA conjugate was labeled with 1 mCi

of ^{64}Cu for 1 h in NH_4Ac buffer (pH = 5.4) followed by PD-10 column purification. ^{64}Cu was produced at NIH by the irradiation of a thin layer of ^{64}Ni (Isoflex, USA) electroplated on a solid gold internal target plate of the CS-30 cyclotron utilizing the nuclear reaction $^{64}Ni(p,n)^{64}Cu$ and separated from the target material as $^{64}CuCl_2$ by anion chromatography.

Gel-filtration chromatography (GFC)

Hydrodynamic diameters (HD) of particles were analyzed by a gel-filtration chromatography (GFC) following a previous report.[5] Calibration of HD was performed by injecting 100 μL protein standards (Bio-Rad, Hercules, CA) containing thyroglobulin (M1, 669 kDa, 18.8 nm HD), γ-globulin (M2, 158 kDa, 11.9 nm HD), ovalbumin (M3, 44 kDa, 6.13 nm HD), myoglobin (M4, 17 kDa, 3.83 nm HD), and vitamin B12 (M5, 1.35 kDa, 1.48 nm HD). To measure whether serum proteins would be adsorbed onto C-dots, 1 mg/mL C-dot-ZW800 were incubated in PBS (pH = 7.4), 95% fetal bovine serum (FBS), or 95% urine for 1 h at 37 °C before loading onto the GFC column.

Tissue sample collection and analysis

Animal procedures were performed according to a protocol approved by the National Institutes of Health Clinical Center Animal Care and Use Committee (NIH CC/ACUC). After the injection of C-dot-ZW800, different organ and tissue samples were collected and analyzed. Briefly, C-dot-ZW800 in PBS solution (2.5 mg/kg, 50 μL) were injected by different routes (n = 4/group): intravenous injection (i.v., tail vein), subcutaneous injection (s.c., under the skin of left leg), and intramuscular injection (i.m., muscle of left leg), respectively. Blood samples (5 μl/withdrawal) were collected from tail vein at different time points (1, 2, 5, 10, 15, 20, 25, 30, 45, and 60 min) postinjection of C-dot-ZW800. The samples were analyzed by a Maestro all-optical imaging system. For the urine clearance analysis, the mice were kept under isoflurane anesthesia (2% v/v isoflurane at 0.2 L min^{-1} O_2 flow) and the bladders of mice were exposed. Subsequently, the bladders were imaged before and after three injection routes at indicated time points. Separate animals were also sacrificed and different organs/tissues were collected at different time points for *ex vivo* fluorescence imaging. NIR fluorescence imaging was acquired by an appropriate filter set for ZW800 (excitation at 685–730 nm, emission at 745–800 nm) on a Maestro all-optical imaging system. The accumulation of particles at injection sites was also studied by exposing injection sites after different routes of injection and then imaged by a Maestro all-optical imaging system.

Tumor inoculation and imaging

The murine squamous cell carcinoma (SCC-7*)* cells were purchased from the American Type Culture Collection (ATCC, Rockville, MD, USA). The cells were maintained in RPMI 1640 medium (Invitrogen) supplemented with 10% FBS at 37°C with 5% CO_2. Flank xenograft tumors were prepared by subcutaneous injection of 10^6 SCC-7 cells suspended in serum free medium into each 5–7 week old female athymic nude mouse. When the diameter of tumors reached about 8 mm, the mice were divided into three groups (n = 4/group), the C-dot-ZW800 particles (2.5 mg/kg, 50 μL) were injected by by intravenous (i.v.), subcutaneous (s.c.) or intramuscular (i.m.) route. The tumor uptake of particles was visualized and quantified by a Maestro all-optical imaging system.

Dynamic PET scans were performed using an Inveon microPET/CTscanner (Siemens Medical Solutions).[45] The dynamic PET data acquisition was started right before the injection (i.v., s.c. or i.m.) of ^{64}Cu-C-dot (100 μCi/mouse, 50 μL). The body temperature of mice was maintained using a thermostat-controlled thermal heater. PET Images were

reconstructed by 2-dimensional ordered-subsets expectation maximum (OSEM) algorithm and the frame rates were 10×30s, 20×60s, 5×120s and 5×300s.

Histological Analysis

Tissue samples were snap-frozen and 5 μm cryosections were prepared to check the biodistribution of particles by Olympus fluorescence microscopy. Specifically, the histology sections were washed twice with PBS and incubated with Z-fix solution for 10 min. Then, the histology sections were stained with 4', 6'-diamidino-2-phenylindole (DAPI) and observed under a fluorescence microscope. The signal derived from C-dots and ZW800 were observed by appropriate filters and software of the fluorescence microscopy (Olympus IX81).

Statistical Analysis

The level of significance in all statistical analyses was set at a probability of $p < 0.05$. Data are presented as mean ± SD. Analysis of variance and *t* tests were used to analyze the data.

Supplementary Material

Refer to Web version on PubMed Central for supplementary material.

Acknowledgments

This work was supported in part, by the National Basic Research Program of China (973 program 2013CB733802), the National Science Foundation of China (NSFC) (81201086, 81201129, 81101101, and 51273165), the Intramural Research Program of the NIBIB, NIH and the Henry M. Jackson Foundation. S.L. was partially supported by an NIH Pathway to Independence (K99/R00) Award.

REFERENCES

1. So MK, Xu C, Loening AM, Gambhir SS, Rao J. Self-Illuminating Quantum Dot Conjugates for *in Vivo* Imaging. Nat. Biotechnol. 2006; 24:339–343. [PubMed: 16501578]
2. Gao X, Cui Y, Levenson RM, Chung LW, Nie S. *In Vivo* Cancer Targeting and Imaging with Semiconductor Quantum Dots. Nat. Biotechnol. 2004; 22:969–976. [PubMed: 15258594]
3. Jaiswal JK, Mattoussi H, Mauro JM, Simon SM. Long-Term Multiple Color Imaging of Live Cells Using Quantum Dot Bioconjugates. Nat. Biotechnol. 2003; 21:47–51. [PubMed: 12459736]
4. Han M, Gao X, Su JZ, Nie S. Quantum-Dot-Tagged Microbeads for Multiplexed Optical Coding of Biomolecules. Nat. Biotechnol. 2001; 19:631–635. [PubMed: 11433273]
5. Cai W, Shin DW, Chen K, Gheysens O, Cao Q, Wang SX, Gambhir SS, Chen X. Peptide-Labeled near-Infrared Quantum Dots for Imaging Tumor Vasculature in Living Subjects. Nano Lett. 2006; 6:669–676. [PubMed: 16608262]
6. Gao J, Chen K, Xie R, Xie J, Lee S, Cheng Z, Peng X, Chen X. Ultrasmall near-Infrared Non-Cadmium Quantum Dots for *in Vivo* Tumor Imaging. Small. 2010; 6:256–261. [PubMed: 19911392]
7. Zhang Y, Wang TH. Quantum Dot Enabled Molecular Sensing and Diagnostics. Theranostics. 2012; 2:631–654. [PubMed: 22916072]
8. Baba K, Nishida K. Single-Molecule Tracking in Living Cells Using Single Quantum Dot Applications. Theranostics. 2012; 2:655–667. [PubMed: 22896768]
9. Li YF, Chen C. Fate and Toxicity of Metallic and Metal-Containing Nanoparticles for Biomedical Applications. Small. 2011; 7:2965–2980. [PubMed: 21932238]
10. Ambrosone A, Mattera L, Marchesano V, Quarta A, Susha AS, Tino A, Rogach AL, Tortiglione C. Mechanisms Underlying Toxicity Induced by Cdte Quantum Dots Determined in an Invertebrate Model Organism. Biomaterials. 2012; 33:1991–2000. [PubMed: 22169823]

11. Chen N, He Y, Su Y, Li X, Huang Q, Wang H, Zhang X, Tai R, Fan C. The Cytotoxicity of Cadmium-Based Quantum Dots. Biomaterials. 2012; 33:1238–1244. [PubMed: 22078811]
12. Yang Y, Zhu H, Colvin VL, Alvarez PJ. Cellular and Transcriptional Response of Pseudomonas Stutzeri to Quantum Dots under Aerobic and Denitrifying Conditions. Environ. Sci. Technol. 2011; 45:4988–4994. [PubMed: 21526814]
13. Clift MJ, Stone V. Quantum Dots: An Insight and Perspective of Their Biological Interaction and How This Relates to Their Relevance for Clinical Use. Theranostics. 2012; 2:668–680. [PubMed: 22896769]
14. Baker SN, Baker GA. Luminescent Carbon Nanodots: Emergent Nanolights. Angew. Chem. Int. Ed. Engl. 2010; 49:6726–6744. [PubMed: 20687055]
15. Fang Y, Guo S, Li D, Zhu C, Ren W, Dong S, Wang E. Easy Synthesis and Imaging Applications of Cross-Linked Green Fluorescent Hollow Carbon Nanoparticles. ACS Nano. 2012; 6:400–409. [PubMed: 22188541]
16. Lu J, Yang JX, Wang J, Lim A, Wang S, Loh KP. One-Pot Synthesis of Fluorescent Carbon Nanoribbons, Nanoparticles, and Graphene by the Exfoliation of Graphite in Ionic Liquids. ACS Nano. 2009; 3:2367–2375. [PubMed: 19702326]
17. Yang Y, Cui J, Zheng M, Hu C, Tan S, Xiao Y, Yang Q, Liu Y. One-Step Synthesis of Amino-Functionalized Fluorescent Carbon Nanoparticles by Hydrothermal Carbonization of Chitosan. Chem. Commun. (Camb.). 2012; 48:380–382. [PubMed: 22080285]
18. Zhu H, Wang X, Li Y, Wang Z, Yang F, Yang X. Microwave Synthesis of Fluorescent Carbon Nanoparticles with Electrochemiluminescence Properties. Chem. Commun. (Camb.). 2009:5118–5120. [PubMed: 20448965]
19. Liu H, Ye T, Mao C. Fluorescent Carbon Nanoparticles Derived from Candle Soot. Angew. Chem. Int. Ed. Engl. 2007; 46:6473–6475. [PubMed: 17645271]
20. Liu R, Wu D, Liu S, Koynov K, Knoll W, Li Q. An Aqueous Route to Multicolor Photoluminescent Carbon Dots Using Silica Spheres as Carriers. Angew. Chem. Int. Ed. Engl. 2009; 48:4598–4601. [PubMed: 19388019]
21. Sun YP, Zhou B, Lin Y, Wang W, Fernando KA, Pathak P, Meziani MJ, Harruff BA, Wang X, Wang H, et al. Quantum-Sized Carbon Dots for Bright and Colorful Photoluminescence. J. Am. Chem. Soc. 2006; 128:7756–7757. [PubMed: 16771487]
22. Cao L, Wang X, Meziani MJ, Lu F, Wang H, Luo PG, Lin Y, Harruff BA, Veca LM, Murray D, et al. Carbon Dots for Multiphoton Bioimaging. J. Am. Chem. Soc. 2007; 129:11318–11319. [PubMed: 17722926]
23. Peng J, Gao W, Gupta BK, Liu Z, Romero-Aburto R, Ge L, Song L, Alemany LB, Zhan X, Gao G, et al. Graphene Quantum Dots Derived from Carbon Fibers. Nano Lett. 2012; 12:844–849. [PubMed: 22216895]
24. Cao L, Yang ST, Wang X, Luo PG, Liu JH, Sahu S, Liu Y, Sun YP. Competitive Performance of Carbon"Quantum" Dots in Optical Bioimaging. Theranostics. 2012; 2:295–301. [PubMed: 22448196]
25. Tao H, Yang K, Ma Z, Wan J, Zhang Y, Kang Z, Liu Z. *In Vivo* NIR Fluorescence Imaging, Biodistribution, and Toxicology of Photoluminescent Carbon Dots Produced from Carbon Nanotubes and Graphite. Small. 2011; 8:281–290.
26. Gao J, Chen K, Luong R, Bouley DM, Mao H, Qiao T, Gambhir SS, Cheng Z. A Novel Clinically Translatable Fluorescent Nanoparticle for Targeted Molecular Imaging of Tumors in Living Subjects. Nano Lett. 2012; 12:281–286. [PubMed: 22172022]
27. Choi HS, Frangioni JV. Nanoparticles for Biomedical Imaging: Fundamentals of Clinical Translation. Mol. Imaging. 2010; 9:291–310. [PubMed: 21084027]
28. Choi HS, Liu W, Misra P, Tanaka E, Zimmer JP, Itty Ipe B, Bawendi MG, Frangioni JV. Renal Clearance of Quantum Dots. Nat. Biotechnol. 2007; 25:1165–1170. [PubMed: 17891134]
29. Choi HS, Ipe BI, Misra P, Lee JH, Bawendi MG, Frangioni JV. Tissue- and Organ-Selective Biodistribution of Nir Fluorescent Quantum Dots. Nano Lett. 2009; 9:2354–2359. [PubMed: 19422261]
30. Choi HS, Liu W, Liu F, Nasr K, Misra P, Bawendi MG, Frangioni JV. Design Considerations for Tumour-Targeted Nanoparticles. Nat. Nanotechnol. 2010; 5:42–47. [PubMed: 19893516]

31. Colvin VL. The Potential Environmental Impact of Engineered Nanomaterials. Nat. Biotechnol. 2003; 21:1166–1170. [PubMed: 14520401]
32. Sarlo K, Blackburn KL, Clark ED, Grothaus J, Chaney J, Neu S, Flood J, Abbott D, Bohne C, Casey K, et al. Tissue Distribution of 20 nm, 100 nm and 1000 nm Fluorescent Polystyrene Latex Nanospheres Following Acute Systemic or Acute and Repeat Airway Exposure in the Rat. Toxicology. 2009; 263:117–126. [PubMed: 19615422]
33. Zhang XD, Wu HY, Wu D, Wang YY, Chang JH, Zhai ZB, Meng AM, Liu PX, Zhang LA, Fan FY. Toxicologic Effects of Gold Nanoparticles *in Vivo* by Different Administration Routes. Int. J. Nanomedicine. 2010; 5:771–781. [PubMed: 21042423]
34. Yang ST, Wang X, Wang H, Lu F, Luo PG, Cao L, Meziani MJ, Liu JH, Liu Y, Chen M, et al. Carbon Dots as Nontoxic and High-Performance Fluorescence Imaging Agents. J. Phys. Chem. C Nanomater. Interfaces. 2009; 113:18110–18114. [PubMed: 20357893]
35. Filonov GS, Piatkevich KD, Ting LM, Zhang J, Kim K, Verkhusha VV. Bright and Stable near-Infrared Fluorescent Protein for *in Vivo* Imaging. Nat. Biotechnol. 2011; 29:757–761. [PubMed: 21765402]
36. Welsher K, Sherlock SP, Dai H. Deep-Tissue Anatomical Imaging of Mice Using Carbon Nanotube Fluorophores in the Second near-Infrared Window. Proc. Natl. Acad. SciUSA. 2011; 108:8943–8948.
37. Smith AM, Mancini MC, Nie S. Bioimaging: Second Window for *in Vivo* Imaging. Nat. Nanotechnol. 2009; 4:710–711. [PubMed: 19898521]
38. Huang P, Lin J, Wang X, Wang Z, Zhang C, He M, Wang K, Chen F, Li Z, Shen G, et al. Light-Triggered Theranostics Based on Photosensitizer-Conjugated Carbon Dots for Simultaneous Enhanced-Fluorescence Imaging and Photodynamic Therapy. Adv. Mater. 2012; 24:5104–5110. [PubMed: 22718562]
39. Choi HS, Nasr K, Alyabyev S, Feith D, Lee JH, Kim SH, Ashitate Y, Hyun H, Patonay G, Strekowski L, et al. Synthesis and *in Vivo* Fate of Zwitterionic Near-Infrared Fluorophores. Angew. Chem. Int. Ed. Engl. 2011; 50:6258–6263. [PubMed: 21656624]
40. Liu W, Choi HS, Zimmer JP, Tanaka E, Frangioni JV, Bawendi M. Compact Cysteine-Coated Cdse(Zncds) Quantum Dots for *in Vivo* Applications. J. Am. Chem. Soc. 2007; 129:14530–14531. [PubMed: 17983223]
41. Huang X, Li L, Liu T, Hao N, Liu H, Chen D, Tang F. The Shape Effect of Mesoporous Silica Nanoparticles on Biodistribution, Clearance, and Biocompatibility *in Vivo*. ACS Nano. 2011; 5:5390–5399. [PubMed: 21634407]
42. Praetner M, Rehberg M, Bihari P, Lerchenberger M, Uhl B, Holzer M, Eichhorn ME, Furst R, Perisic T, Reichel CA, et al. The Contribution of the Capillary Endothelium to Blood Clearance and Tissue Deposition of Anionic Quantum Dots *in Vivo*. Biomaterials. 2010; 31:6692–6700. [PubMed: 20619783]
43. Kunjachan S, Gremse F, Theek B, Koczera P, Pola R, Pechar M, Etrych T, Ulbrich K, Storm G, Kiessling F, et al. Noninvasive Optical Imaging of Nanomedicine Biodistribution. ACS Nano. 2013; 7:252–262. [PubMed: 23067565]
44. Yang ST, Cao L, Luo PG, Lu F, Wang X, Wang H, Meziani MJ, Liu Y, Qi G, Sun YP. Carbon Dots for Optical Imaging *in Vivo*. J. Am Chem. Soc. 2009; 131:11308–11309. [PubMed: 19722643]
45. Zhu L, Guo N, Li Q, Ma Y, Jacboson O, Lee S, Choi HS, Mansfield JR, Niu G, Chen X. Dynamic Pet and Optical Imaging and Compartment Modeling Using a Dual-Labeled Cyclic Rgd Peptide Probe. Theranostics. 2012; 2:746–756. [PubMed: 22916074]

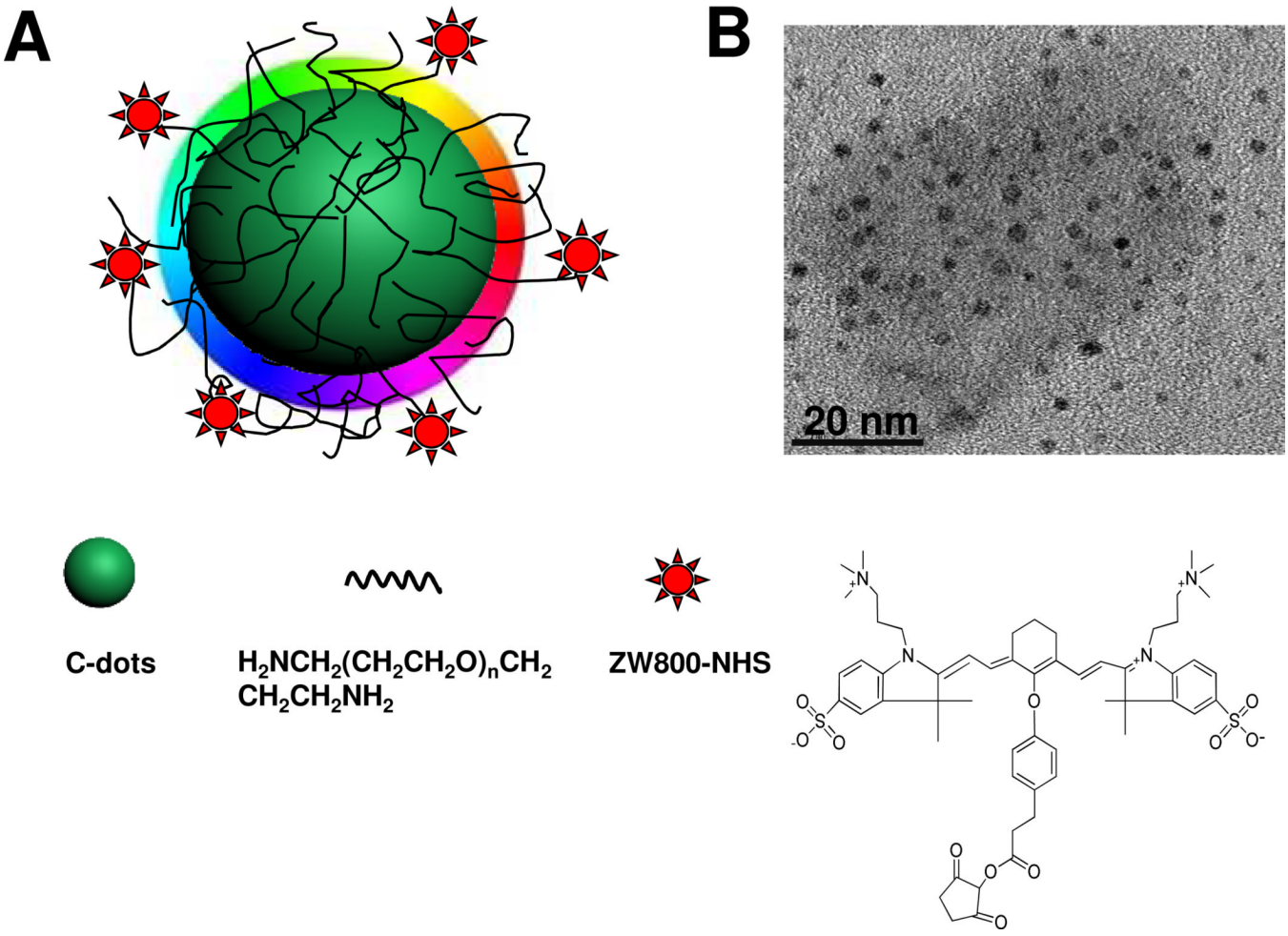

Figure 1.
(A) Schematic structure of C-dot-ZW800 conjugate. (B) TEM image of C-dots.

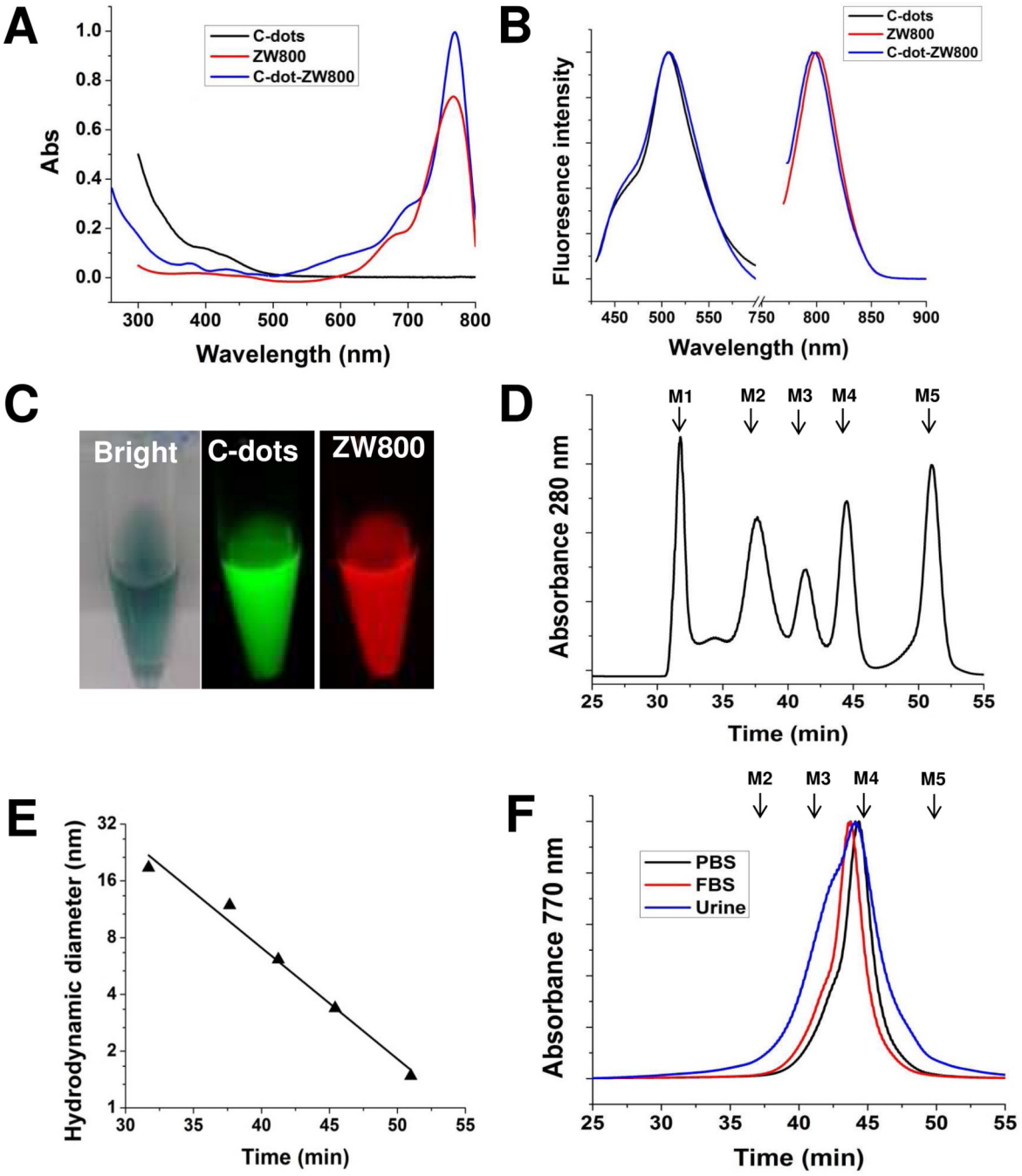

Figure 2.

Optical properties and hydrodynamic diameters (HD) of C-dot-ZW800. Representative (A) absorbance and (B) fluorescence emission (λ_{Ex} = 420, 770 nm) spectra of C-dots, ZW800 and C-dot-ZW800. (C) Fluorescence images of C-dot-ZW800 based on C-dots and ZW800 by a Maestro imaging system, respectively. (D) Gel-filtration chromatography (GFC) analysis of protein standards (PBS, pH = 7.4). Molecular weight markers M1 (thyroglobulin; 669 kDa, 18.8 nm HD), M2 (γ-globulin; 158 kDa, 11.9 nm HD), M3 (ovalbumin; 44 kDa, 6.13 nm HD), M4 (myoglobin; 17 kDa, 3.83 nm HD), and M5 (vitamin B12; 1.35 kDa, 1.48 nm HD) are shown by arrows. The retention time of protein standards at absorbance of 280 nm was analyzed by reversed-phase HPLC. (E) GFC standard curve between HD and

retention time. (F) Stability of C-dot-ZW800 in PBS, FBS and urine after 1 h incubation at 37 °C prior to loading onto the GFC column. The retention time of particles at absorbance of 770 nm was analyzed by reversed-phase HPLC.

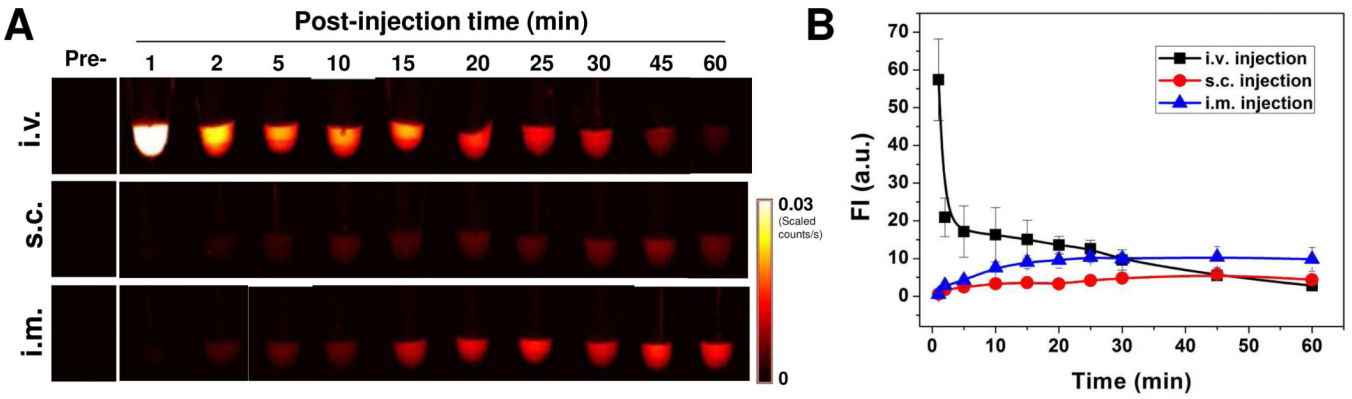

Figure 3.

Blood circulation of C-dot-ZW800 after three injection routes. (A) After injection of particles, vein blood samples (5 μL) at indicated time points were collected into Eppendorf tubes containing 5 μL heparin solution, and subsequently NIR fluorescence images were acquired. (Top) i.v. injection, (Middle) s.c. injection, and (Bottom) i.m. injection. (B) Fluorescence time-activity curves derived from signals in (A).

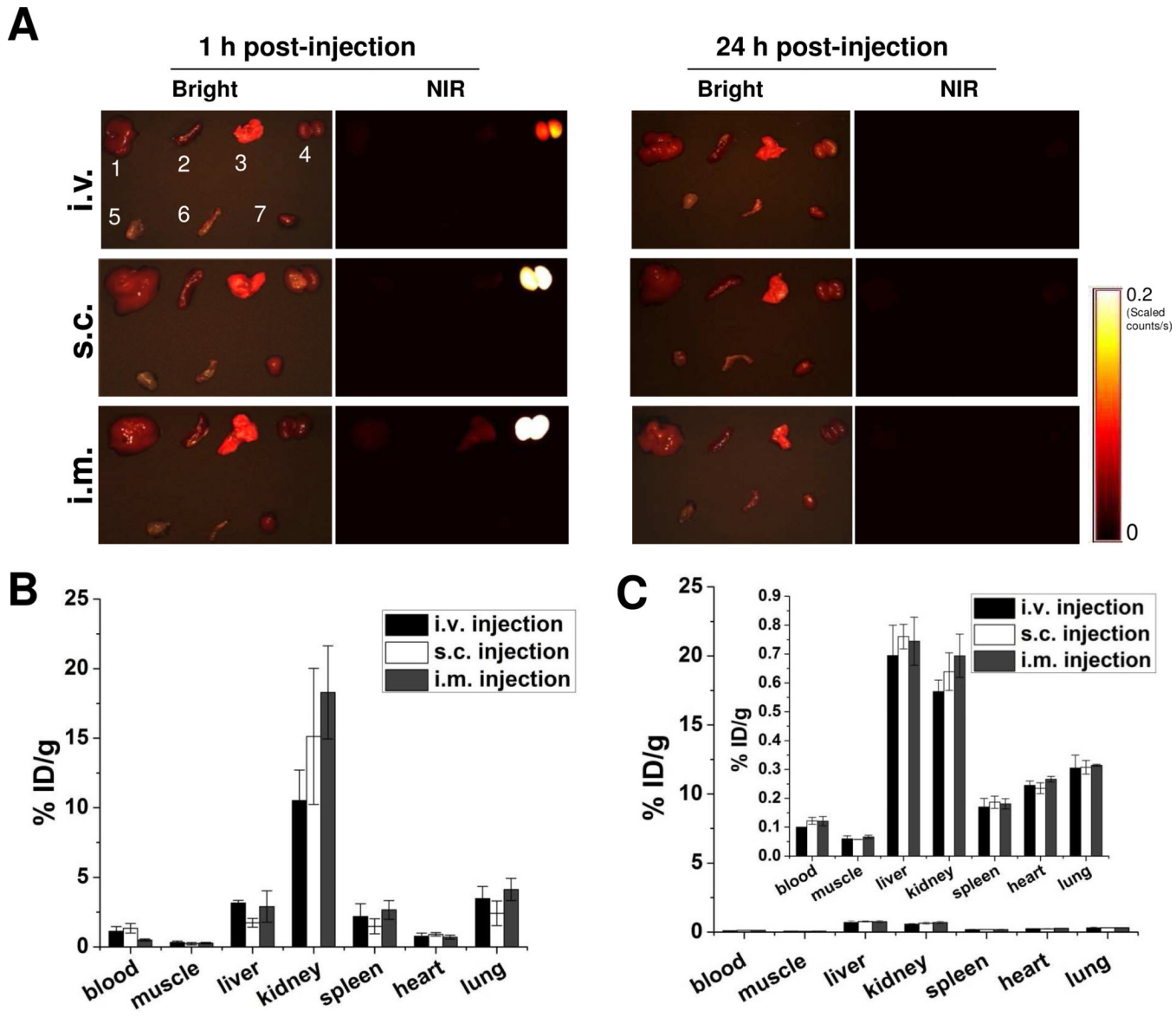

Figure 4.

Biodistribution of particles after three injection routes. (A) *Ex vivo* imaging of biodistribution of C-dot particles. After injection of particles, the major organs and tissues were harvested from Balb/C mice at the indicated time points, and subsequently, the bright field and NIR imaging were acquired using a Maestro imaging system. Left, 1 h post-injection (top, i.v.; middle, s.c.; bottom, i.m.); right, 24 h post-injection (top, i.v.; middle, s.c.; bottom, i.m.). Bright field: 1, liver; 2, spleen; 3, lung; 4, kidneys; 5, muscle; 6, intestine; 7, heart. (B-C) Quantification of the biodistribution of ^{64}Cu labeled C-dots *via* three injection routes at 1 h (B) and 24 h (C) time points. At 1 h and 24 h postinjection of ^{64}Cu-C-dot, the mice were euthanized and major organs and tissues including blood, muscle, liver, kidneys, spleen, heart and lung were harvested and measured by gamma counting.

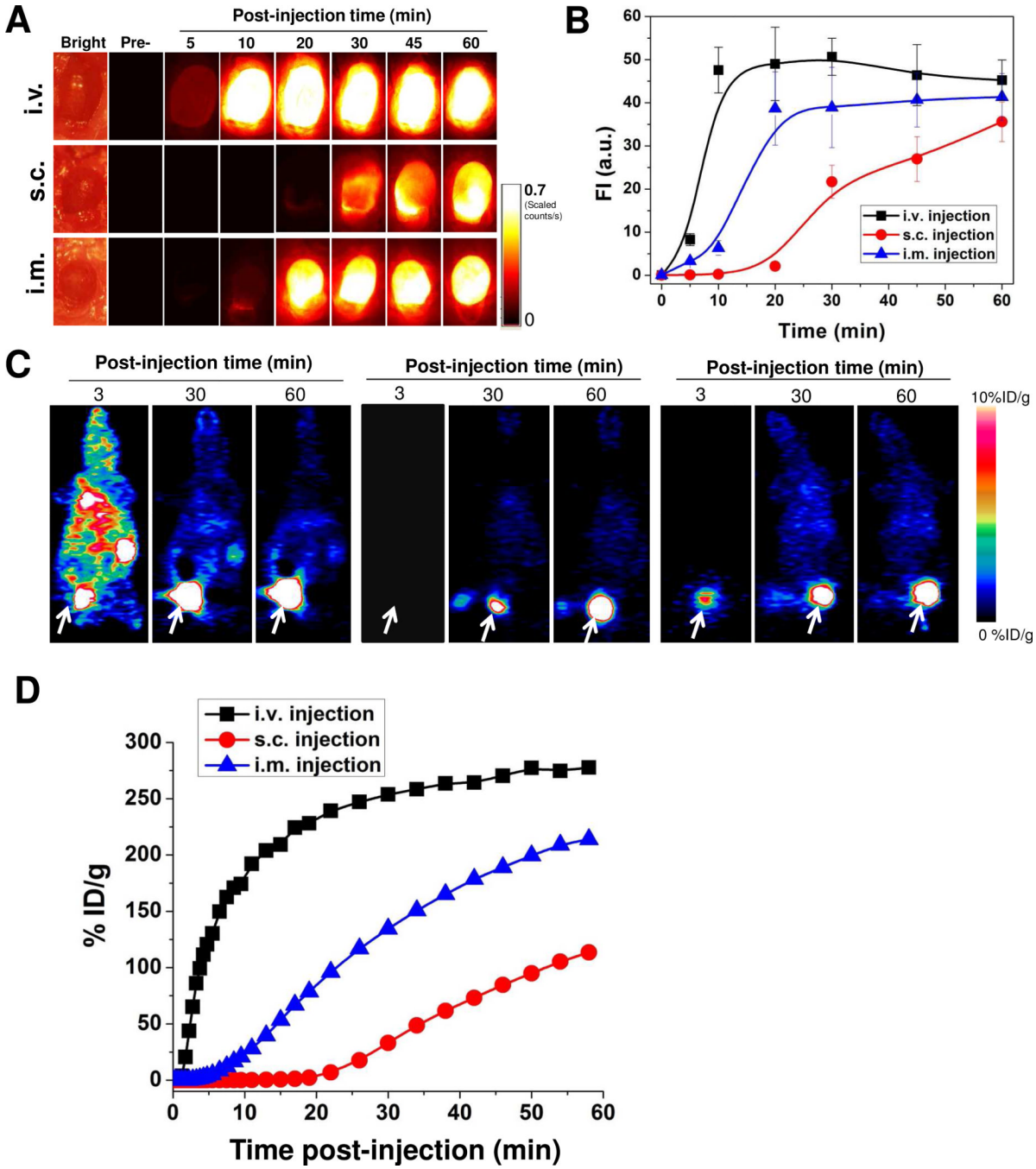

Figure 5.

Urine accumulation of C-dot-ZW800 after different routes of injection. (A) The mice were kept under isoflurane anesthesia and the bladder was exposed and NIR images were acquired at the indicated time points before and after (top) i.v. injection, (middle) s.c. injection and (bottom) i.m. injection. (B) Quantification of the ZW800 fluorescence signal in (A). (C) Representative coronal images from 1 h dynamic PET imaging of ^{64}Cu-C-dot after three routes of injection: left, i.v. injection; middle, s.c. injection; right, i.m. injection. (D) Urinary bladder ROI analysis of the PET images in (C).

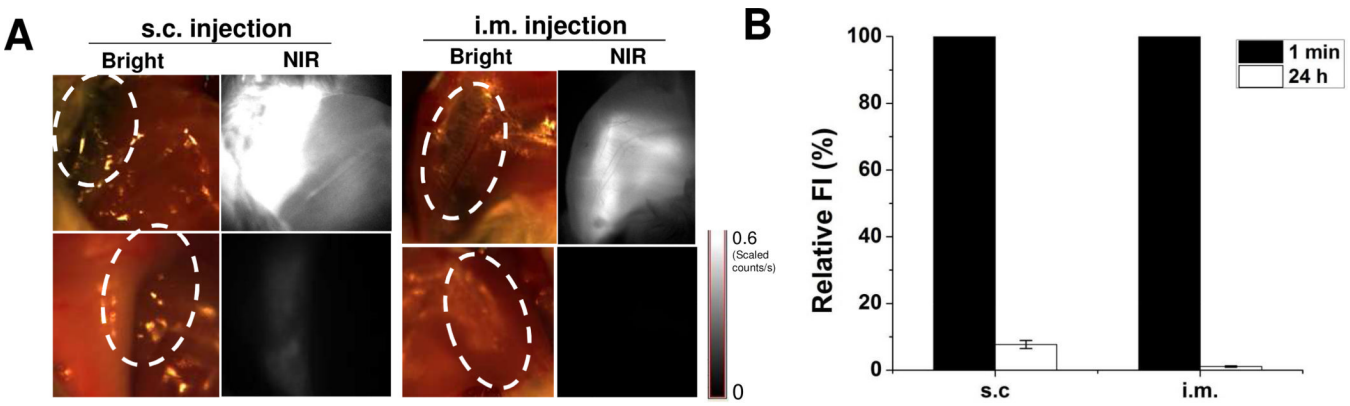

Figure 6.

Accumulation of C-dot-ZW800 at s.c. and i.m. injection sites. (A) NIR fluorescence images at (top) 1 min and (bottom) 24 h after s.c. injection and i.m. injection: left, bright field images; right, NIR fluorescence images. The injection sites are indicated by circles. (B) Quantification of the relative fluorescence intensity at the injection sites over time.

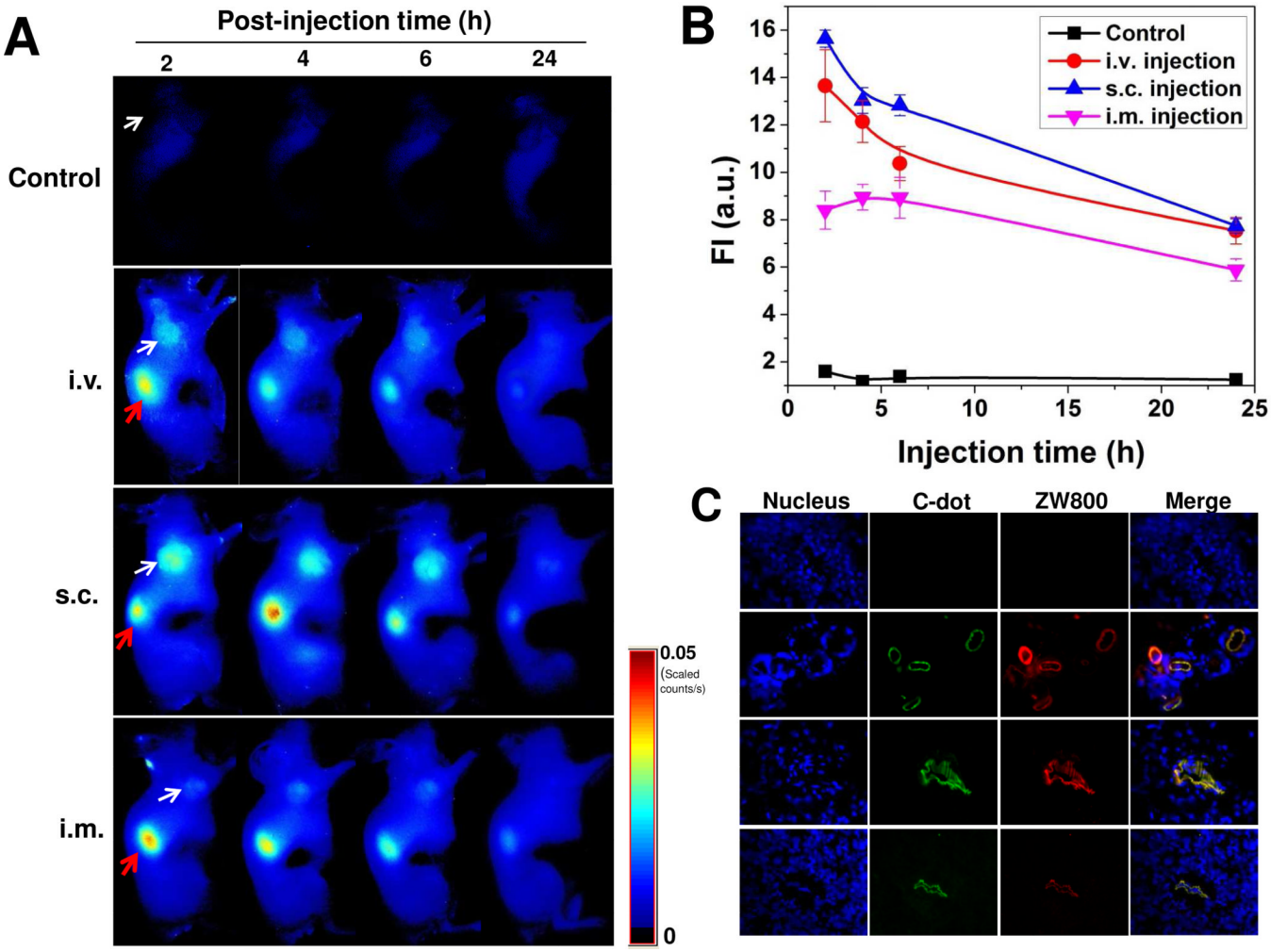

Figure 7.

Tumor uptake of C-dot-ZW800 after different routes of injection. (A) NIR fluorescence images of SCC-7 tumor-bearing mice acquired at 2, 4, 6 and 24 h postinjection: control (without injection), i.v. injection; s.c. injection; i.m. injection (white arrow indicates tumor; red arrow indicates kidney). (B) Tumor ROI analysis. Fluorescence signal unit: $\times 10^8$ photons/cm^2/s. (C) *Ex vivo* fluorescence images derived from the emission of C-dots and ZW800 were acquired to confirm tumor uptake of particles.